The Stable distribution as a physically meaningful description of the size distribution from Rayleigh resonance jet break up type atomisers

P. Threlfall-Holmes*
* Complex Fluids and Colloid Science Expert Capability Group
AkzoNobel Research, Development and Innovation
Wilton Centre, Redcar. TS10 4RF UK

Abstract

During the development of an atomiser working on the principle of Rayleigh resonance jet break up for industrial scale spray drying, it was found that the narrow droplet size distribution from this "Acoustic Atomiser" was inadequately described by the distribution functions commonly used for sprays, but well described by the Stable distribution. The alpha parameter of this distribution was found to tend towards the Gaussian limit for low viscosity fluids and the Lorentz limit with increasing viscosity, consistent with behaviour as a simple and damped forced harmonic oscillator respectively, and hence with the physics of the atomisation process.

Introduction

Spray dryers are equipment that are widely used in the process, food and pharmaceutical industries for the conversion of bulk liquid into dry powder products by evaporation of a liquid solvent, particularly for heat sensitive products such as pharmaceuticals and foods, especially coffee and dairy products [1-4].

Atomisers in spray dryers are normally either rotary atomisers, pressure nozzles, or two-fluid nozzles [1], all of which create a wide distribution of droplet sizes. A spray dryer must have sufficient residence time to solidify the largest drops, otherwise they will be deposited on the inside surfaces of the chamber, especially at the base. Not only are chamber deposits inefficient loss of product, they also increase fire and explosion risk, limit the on-line time between cleanouts, and make cleaning more arduous. In order to ensure that the large diameter tail of the droplet distribution is dry within the residence time of a drying chamber of economically constructible and operable size, it is typically necessary to make a rather fine powder, in the range 50-100μm mean diameter. Consequently, the smallest droplets in the size distribution dry to dust. If directly harvested as product, dust makes the powder more difficult to handle, both by reducing flowability, and also due to the greater controls required to protect personnel from respirable sub-10μm dust. The dust may need to be recycled back into the feedstock, or into the atomisation zone, as nuclei to promote agglomeration within the spray dryer. Dust is the fraction most sensitive to ignition, due to the very high specific surface area, hence increasing the explosion risk.

Post-spray drying granulation is frequently a pragmatic necessity in order to increase the particle size to some hundreds of micrometre diameter, and hence to confer desirable properties such as flowability and re-dispersibility to the powder. The granulation step increases both the capital and operating costs of the powder production plant. It is also something of a "black-art", relying on operator experience for design and operation, rather than on robust predictive models. In consequence most spray drying operations have two series-coupled unit operations, the fundamentals of each of which are rather poorly understood.

The largest droplets in the size distribution have the greatest terminal velocity, hence the least residence time in the spray dryer, but require the greatest residence time to dry or solidify. Since these largest droplets determine the overall dryer residence time, the majority of droplets have a residence time much larger than is required for solidification. In spray drying, the sensible heat of the dry particle is normally tiny compared with the latent heat of the evaporation of water, so the effect of increased residence time is to heat up the dry particle significantly, risking the very heat degradation which is intended to be avoided by the short spray dryer residence time. In practice, a balance is struck (although it is not normally articulated explicitly by plant operators), averaging out the final moisture content and heat degradation across the size distribution.

Whilst commercial spray dried products have for decades been made with the compromises engendered by wide size distribution atomisers, it would appear reasonable to expect potential for enhanced process efficiency and improved products using a atomiser producing a narrow droplet size distribution. ICI (now a wholly owned subsidiary of AkzoNobel) developed atomisers for spray drying and prilling (spray-solidification of melts) which exploit the Raleigh laminar jet resonance instability [5, 6] to produce droplets which are all of substantially the same size [7, 8]. When a varicose liquid jet is vibrated at its natural (resonant) frequency, surface waves at this frequency are propagated along the jet, increasing in amplitude until they neck off uniform sized droplets from the jet.

* Corresponding author: phil.threlfall-holmes@akzonobel.com

In practice it has been found that the difference in spray dried product quality when using the Rayleigh resonance jet break up "Acoustic Atomiser" is surprisingly dramatic [9, 10]. At ILASS-Europe 2004, I reported a droplet residence time scaling analysis which rationalises why the product becomes so much more uniform [11]. That preliminary version of the analysis used a log-normal distribution as a model for the droplet size distribution, based on fits to powder product sieve sizing data. The residence time scaling analysis is based on matching the 95^{th}-99^{th} percentile of the droplet size distribution, so to have confidence in that analysis, the size distribution model should be a very good fit to the data. In the research reported here, considering a wider range of size distribution data sources, it was found that the log-normal distribution was not a satisfactory fit to all the data. In particular, the tails are not well fitted: using statistical tools the tail behaviour is shown to be deviant even for the fit to the data which were the original reference. Since the physics of atomisation are not completely understood, it is not the normal expectation to be able to select an appropriate function a priori, and a selection of likely alternatives were tested. It was found that the best fits were obtained with the Stable distribution. This has not previously been reported to be applicable to spray size distributions. Surprisingly, there appears to be some scientific rational for the values of the Stable parameters. The alpha parameter of this distribution was found to tend towards the Gaussian limit for low viscosity fluids and the Lorentz limit with increasing viscosity, consistent with the physical behaviour of the atomiser as a simple and damped forced harmonic oscillator respectively.

Droplet size distribution data sources

The 40 Acoustic Atomiser droplet size distribution datasets fitted in this research cover a variety of materials, spray-dried and spray-cooled, with mean sizes varying over two orders of magnitude and flowrate ranging over four orders of magnitude. The data have been measured by Phase Doppler Anemometry (PDA), image analysis and sieve sizing. A few datasets are measurements of liquid droplet size, but most are measurements of solid particle product, i.e. incorporating dispersion in particle size due to morphology and size changes during solidification, as well as due to variations in droplet size from the atomiser. Whilst the datasets are thus individually rather noisy, we can be confident in the robustness of a fit to such a range of data. The sources are described in the following sub-sections: the complete data can be found in [12]. The specific materials used are immaterial to the science of the size distributions, and to protect commercial confidentiality, apart from the water measurement the materials are not named but listed as A, B, C and D.

Only data where the Acoustic Atomiser was running normally in steady state have been selected. Each dataset is a group of one or more individual determinations of size distribution at a given operating condition. If the sprayhead were truly in steady state, each individual determination of size distribution in any dataset would be a sample of the same time-invariant population. Hence the fit has been performed on the ensemble average of the data in each dataset. Especially for the larger datasets, fitting to each and every determination would not only be computationally intensive, but detract from the purpose, which is to clarify from the mass of experimental size distribution data, a single fit curve which is characteristic of this type of atomiser. Point checks of the expectation of time-invariance were made by visual comparison on the delta stabilised probability plot (described later), that fits to selected individual determinations were the same as fits to the ensemble average for the dataset. An example is plotted in Figure 2. In principle it would be possible to demonstrate quantitatively the time invariance of the realisations within the dataset using the 2-sample Kolmogorov-Smirnov test [13] to test for confidence that two fitted sample size distributions came from the same population. In practice in this instance it would not improve the reliability of the inference about time invariance. The datasets with multiple realisations are all by sieve-sizing or PDA, with only a small number of datapoints in each realisation, and hence large acceptance bands on the 2-sample Kolmogorov-Smirnov statistic. In this circumstance, the visual check of similarity is just as precise.

Water

A single laminar jet of water was measured by Phase Doppler Anemometry (AEA Technology PD Lisatek). The point of intersection of the beams in this instrument is quite small, roughly $1mm^3$, so the measurement is of droplets in the stream issuing from a single jet. To obtain the size distribution from a whole sprayhead would require traversing the head so that each jet in turn was in the probed volume.

The PDA instrument measures a number distribution, in discrete diameter bins rather than continuous. The droplet size distribution peaks from a single resonant nozzle are very sharp, and this PDA is an old design, so the bins are not as finely spaced as would be ideal for resolution of the shape of the peak. However, the spacing of the bins is sufficiently fine that there is little error in the instrument's conversion to volume distribution using the upper limit diameter of the bin, and it is volume distribution data which have been chosen, as this is the natural representation of data from sieve sizing, which is not only the most abundant source of size data for the Acoustic Atomiser, but also is discretised rather coarsely, so the alternative strategy of conversion of sieve sizing data to a number distribution for comparison with PDA data would create serious error.

Spray-cooled materials A and B

Three datasets are sieve size data for a spray-cooled product Material A made in production plants operating at between 60 and 80te/hr. Dataset A1 is an ensemble average of seven size distributions, each from a sample collected at approximately half-hourly intervals during a commissioning trial. Datasets A2 and A3 are ensemble averages of daily production log sieve sizings from two different plants, each covering a month of operation.

Dataset B is an ensemble average of sieve size data from two samples of spray-cooled product Material B, collected at different times during a trial on a 2kg/hr pilot tower at ICI Wilton.

Spray-dried material C

Material C was a spray-dried product, but the size distribution data are of the liquid droplets in the spray using PDA. Datasets C1 and C2 are measurements made on single nozzles, C3 is the cumulative droplet volume distribution curve from a 1 te/hr Acoustic Atomiser. The original PDA frequency data tables are not available for dataset C3, and the data have been digitised from the secondary source of the plotted graph.

Spray-dried materials D

Materials D are spray-dried powder products made in a pilot spray dryer at ICI Wilton at 1-5kg/hr. Powder product size distribution was measured for some samples by sieve, and for others by image analysis (Oxford Lasers Visisize).

In the image analysis sizing, powder was fed from a hopper using a vibrated feeder, tuning the vibration amplitude so that the flow of powder through the field of view of the instrument was maintained sufficiently dilute that individual particles could be properly resolved. The image analysis algorithm in the instrument software determines an area and a perimeter of the objects passing through the field of view, with corrections and rejections for various artefacts such as out of focus objects and dust spots on the lens. The diameter of an equivalent circle is calculated from the area. The area and the perimeter together can be used to test the assumption of sphericity, in a shape factor defined in (1) which is the ratio of the perimeter of an area-equivalent circle to the measured perimeter. Most of the datasets were filtered for gross non-circularity during acquisition. A further analysis of non-circularity has been carried out, see later sub-section on the agglomeration artefact.

$$\text{circularity} = \frac{2\sqrt{\pi.\text{Area}}}{\text{Perimeter}} \tag{1}$$

The Visisize instrument creates a count of particles as a function of their area. As with the PDA data, this number distribution has been transformed into a volume distribution. The original Visisize datafiles were available electronically, so the conversion to volume could be made directly on the 0.1µm precision to which the diameter data was computed by the instrument. Hence there is negligible loss in precision through the transform. With the lens and camera used for these measurements, the calibrated resolution is 7µm/pixel, with a minimum resolvable diameter of 30µm. The loss in precision in the transform from a number to a volume distribution is an order of magnitude less than the inherent resolution accuracy of the data, even in the fine droplet tail where the quantisation by pixilation of area and perimeter measurements is most severe.

The number distribution is quantised by discrete number counts at a diameter increment. These horizontal bands in the number distribution plot become cubic curved bands in the volume distribution plot (see Figure 3 top left plot): these are not a reprographic artefact. Each point on these frequency plots represents the frequency at a 0.1µm diameter increment. There may be many empty size bins between each plotted point, which is not apparent on the full range axes due to finite printable and visible line width compared with bin width. The empty bins need not confound numerical fitting algorithms, hence numerical fits have been made to this unprocessed data. However, the visual impression of the scatter of the volume frequency spectra is erroneous. Hence to depict the goodness-of-fit of theoretical distribution curves to these data, they have also been plotted as histograms, where the bin size was manually iterated until it was sufficiently large that spurious peaks of noise disappeared but the underlying shape of the distribution was not lost. Bins were typically a fixed width of a few µm, up to typically 120% of the fiftieth percentile of the volume distribution (d_{v50}), and thereafter the bins were linearly increased in bin width, typically to 10-20µm width at maximum diameter. It is emphasised that this is purely to aid visual evaluation of fit curves, and the arbitrary histogram bin size is hence defensible.

Droplet size distribution artefacts

Steady satellite droplet formation

When the driving frequency for jet break-up is not quite at resonance a small satellite droplet can form between each main droplet [14]. The breakup still appears to be uniform under strobe lighting. The satellite droplets are small. In the materials D spray drying experiments, the jets were imaged with a low resolution CCD camera, through a sight glass and across the body of the spray dryer. Hence it is understandable that the operator

could not always observe the satellite droplet formation and tune them out. However, the consequence of steady satellite formation is that some of the particle size distributions are bimodal. Satellite droplets can also occur in viscoelastic liquids by a different mechanism, from the collapse of "beads-on-a-string" structures [15]. These persist for sufficient jet length to have been large enough structures to have been visible to the operator, so are a less credible explanation for the bimodal product size distributions in these experiments.

Orifice size variation

Multiple peaks that are too similar in peak location and volume fraction to be satisfactorily explained as satellite droplet peaks can be observed in a number of the materials D datasets. The Acoustic Atomiser used in these experiments had orifices in removable inserts, so that the diameter, number and patternation of the orifices could be varied between experiments. Inconsistency in the orifice diameters fitted to the atomiser is the most likely explanation for the multiple peaks. The manufacturing tolerance on the diameter of the orifice in the inserts was not always as tight as would be desirable. Great care was taken to segregate orifices of different diameters, but it is also possible that sets of orifices of different sizes were mixed up.

Agglomeration

Some agglomeration was observed in many of the spray-dried materials D, either by visual examination of the product in the powder collection bucket or by examination under a microscope. These agglomerates appeared to be composed of discrete particles stuck together, rather than a fused mass. This strongly suggests that agglomerates formed during the late stages of drying, from solid but still sticky particles, rather than from wet liquid droplets. The presence of agglomerates indicates that the powder may not have been fully dry. The result of agglomerates in the product is noisy scattered tertiary peaks in the droplet size distribution at large sizes. As it occurs at large sizes, the data scatter from agglomeration appears large in a volume distribution, even when the number of agglomerates in the sample was small.

It was not possible to use asphericity to filter out the agglomerate artefacts in the Visisize. In all cases it was found that whilst the range of asphericity varied between samples, in any one sample the range of particle asphericity was almost independent of diameter, even when the presence of agglomerates was recorded in the experimental log. That is, for each sample, the primary particles cover as great a range of asymmetry as do the agglomerates, so the shape factor could not be used to filter out agglomerate artefacts in the size distribution.

Determining goodness-of-fit

The goodness-of-fit of the distribution functions to the data was tested by visual comparison on the volume density, the cumulative volume, and a delta stabilised probability (DSP) plot. This latter presentation is derived from the stabilised probability (SP) plot of the cumulative data against the value for corresponding diameter predicted by the cumulative fit function, where both the data and fit probabilities are scaled according to (2), where p is the probability value and sp the scaled value.

$$sp = \frac{2}{\pi}\sin^{-1}\left(\sqrt{p}\right) \tag{2}$$

This transformation makes the variance more uniform across the distribution, and hence is a much more sensitive test of fit to the tails than a standard probability-probability (p-p) plot [16, 17]. If the distribution function tested were a perfect model for the data, the plotted points would all lie on the x = y line. Thus it is straightforward to evaluate goodness-of-fit visually from the SP plot. In addition, a goodness-of-fit statistic D_{SP} has been defined [16]: analogous to the Kolmogorov-Smirnov statistic for a standard p-p plot, it is the maximum deviation of the data from the theoretical fit. This statistic can be tested against confidence limits, which depend only on the sample size, not upon the form of the distribution being tested [13]. This has the huge advantage that the goodness-of-fit statistic can directly be compared between fits of different theoretical distributions to the same dataset. The 95% confidence limits have also been plotted, to further facilitate the visual evaluation of goodness-of-fit.

Michael [16] only computes the confidence limits up to a sample size of 100, whilst the Visisize data have ten thousand samples. There are no literature tabulations of the limits for large samples, and the method Michael describes for the computation of the confidence intervals is daunting. The pragmatic approach of extrapolating from a curve fit to Michael's tabulated values has been adopted. Even though the extrapolation curve fit is very near perfect to the precision of Michael's tabulated data, such gross extrapolation is of course conjecture, and it incorrectly asymptotes to D_{sp} = 0.0548 rather than zero as $n \to \infty$. It is fit for the purpose of discriminating between the various theoretical distributions tested, but it is wise to be especially cautious when the test statistic for the Visisize datasets is close to the confidence limit. Such caution is anyway recommended for the Kolmogorov-Smirnov test on which the DSP test is based [18].

Most of the area in the SP plot is unused, and it is hard to magnify the area of interest around the perfect fit line. Visual assessment of goodness-of-fit is further enhanced in the delta stabilised probability (DSP) plot, where the deviation of the data from the theoretical fit is plotted against the theoretical fit. In the DSP plot the perfect fit line is y = 0 and the acceptance bounds become horizontal. Figure 1 is an example of the DSP plot.

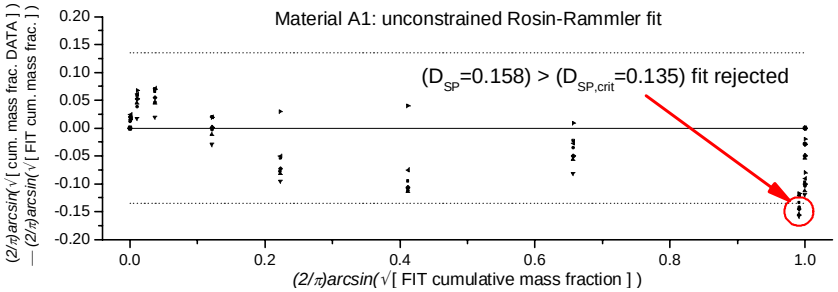

Figure 1. example of the delta stabilised probability (DSP) plot

Droplet size distribution function screening

The distribution functions screened include those used for sprays analysis in the literature, either commonly (log-normal and Rosin-Rammler), or rarely (hyperbolic), and also functions not seen in the sprays literature but which appeared to have a potentially appropriate peak shape (Laplace, Lorentz/Stable, log-logistic/ Burr).

Screening the fit functions was made more complex by the variable quality of the experimental data. The high resolution of the image analysis datasets most clearly show the shape of the primary peak, but in all these datasets there are secondary peaks which mask the tails of the primary distribution. The sieve sizing data for materials A and B are unimodal, but the diameter resolution is low, so the peak shape and kurtosis are not well defined. The PDA data for water and material C have such sharp peaks that the diameter resolution is low, even though the bin size is fine. To be sure that the distribution function was satisfactory, it was necessary to test it across various datasets, in order to check goodness-of-fit to both peak and tails. For the initial screening, five datasets were chosen as representative of the range of sources, and showing the features of the primary peak at as high a resolution as the measurement technique permitted, with as small secondary peaks as possible. Only the theoretical distributions which performed satisfactorily in this initial screening test were fitted to other datasets.

For speed in the initial screening, volume distributions normalised by the total volume were used, i.e. including any secondary peaks where present. This is ultimately inadequate: a good fit to the primary peak is impossible if both data and fit are normalised, but there is an appreciable volume fraction of the data in secondary peaks. With distribution functions which appeared on preliminary screening to be about the right shape, the volume fraction in the primary peak of the data was corrected by an iterative procedure using the fit function. Confining the fit to just the primary peak data is based on the assumption that the secondary peaks arise from ascribable physical phenomena and are not part of the primary atomisation distribution. The validity of this assumption was tested by performing bimodal fitting on the secondary peak ascribed to satellite droplets.

The Non-Linear Curve Fitting tool (NLFit) in Origin 8 (OriginLab Corp.) was used for the monomodal fits. NLFit minimises the chi-squared deviations of the fit curve from the experimental points. Multimodal fitting is possible for many of the NLFit library functions, but excessively complex to code for novel function definitions, so for the bimodal fits, and also for the monomodal Stable distribution fitting, an Excel spreadsheet was used to iterate distribution parameters to minimise D_{SP}, with in the case of the Stable distribution, a Visual Basic macro calling Nolan's "STABLE" FORTRAN program [19] to calculate the Stable densities and cumulative function.

Results from fit function screening

Considering Figure 2, the log-normal distribution appears from the cumulative distribution plot to be a reasonable fit to be the Material B data. However the DSP plot reveals deviation in the tails. In Figure 3 it can be seen that the log-normal distribution fails to capture the peak shape correctly for the Visisize data, and both tails are too narrow. As described earlier, the numerical fitting has been made to unbinned data (Figure 3 top left plot), but the fits are also shown on binned data (top right plot) for convenient visual assessment of the fit.

The log-logistic and its extension, the Burr distribution, were both found to be no more satisfactory fits to the data than the log-normal. The Rosin-Rammler was less good (Figure 1). The Laplace and Lorentz distributions are symmetrical about the mean, and hence unlikely to ultimately be the best fits to the right skewed size distribution data. However, not only are the peak shapes credible, the hyperbolic distribution is a superclass which includes the Laplace distribution as an instance, and the Stable distribution includes the Lorentz as an instance. The promising fits to the data of the computationally simple Laplace and Lorentz distributions indicated that it was worth tackling the complexities of the more computationally complex generalised forms.

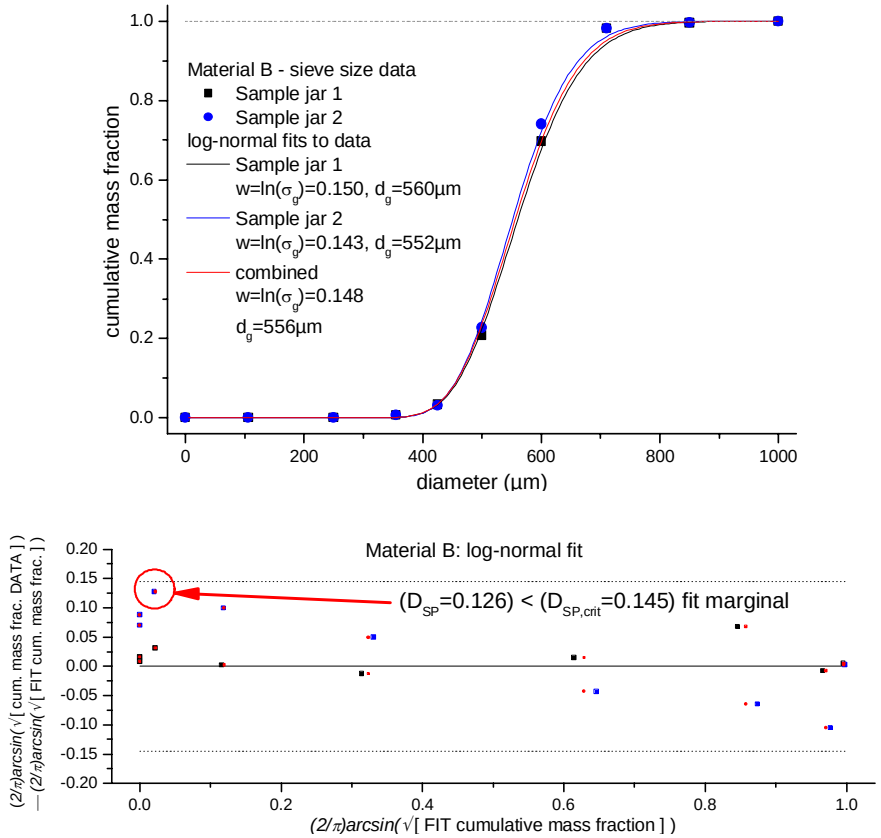

Figure 2. log-normal fits to material B sieve size distribution data

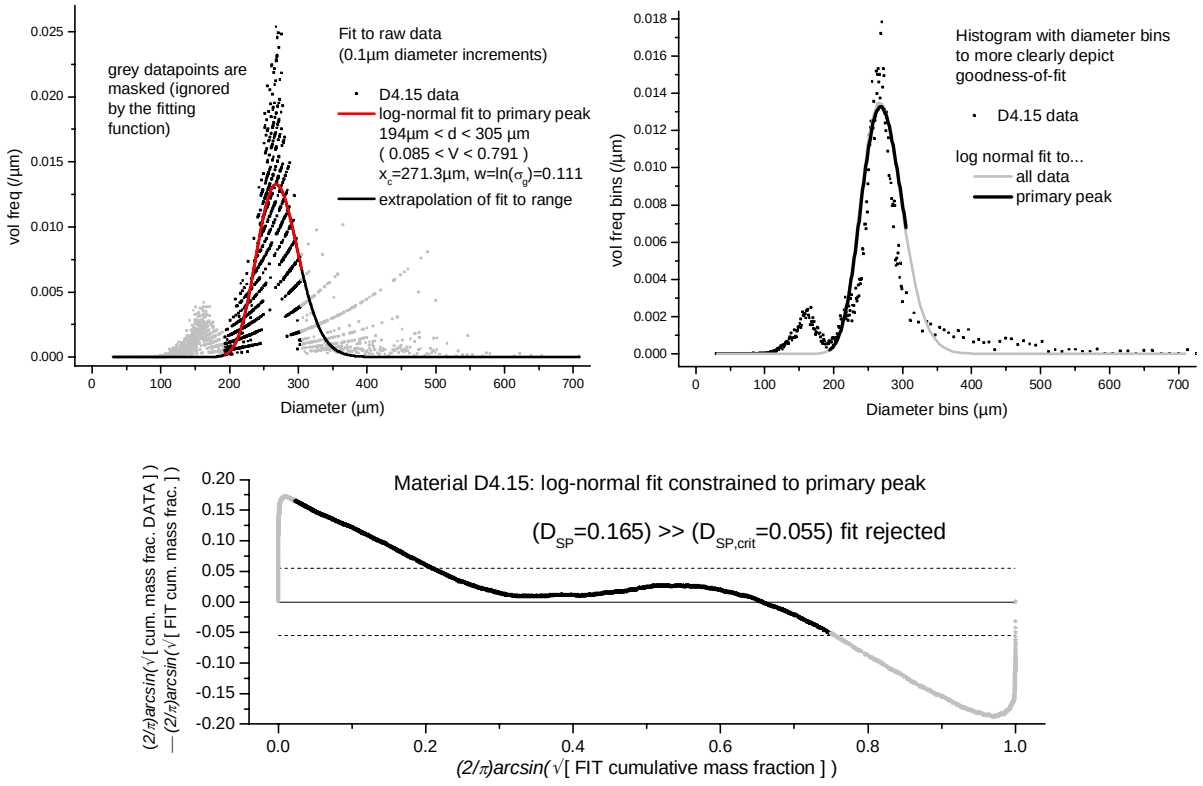

Figure 3. log-normal fits to Visisize dataset D4.15

The hyperbolic distribution

The three and four parameter log-hyperbolic distributions have been shown to be a good fit to spray size distributions [20, 21], although they appear not to be widely used. This is probably due to a combination of the mathematical complexity and the computational effort and instability of fitting. Xu et al. [21] have shown that for the 4-parameter log-hyperbolic (4P-LH) distribution, with the likely accuracy of spray size data, the δ scale parameter is so dominant at the distribution tails that the distribution can be well fitted with arbitrary combinations of the α parameter and the β asymmetry parameter. Although this does not allow for easy comparison of parameters between fits to different datasets, it is an inconvenience rather than a fatal weakness. If the fit is good, some statistics of the distributions, for example the moments, could be computed and compared between datasets as proxies for the distribution parameters. Xu et al. [21] propose an alternative three parameter log-hyperbolic distribution which does not exhibit the parameter instability. Screening datasets were found not to lie within the reduced parameter space of this distribution, and hence it was not considered further.

The fitting was found to be more stable than the literature would suggest, repeatably converging to the same parameters for a given input dataset. The location parameter μ was simply and well estimated as the mode diameter by inspection of the frequency plot of the data. Convergence was stable for any reasonable initial guess for the α, β and δ parameters of the distribution, provided that μ was initially held fixed at this estimated mode diameter whilst good estimates for α, β and δ were computed by the NLFit least squares fit algorithm.

However, in contrast to other distribution functions tested, the fit to the whole dataset was clearly different to the fit to just the primary peak, both in the shape and the values of the parameters: the fit is undesirably sensitive to the selection of the data range. Nor was any pattern apparent in the values of the parameters between datasets: it was not possible to choose a parameter set characteristic for the atomiser. The least squares calculated error in the α, β and μ parameters was satisfactorily small, but the error in δ was found to be up to 2δ, which is most unsatisfactory. The screening test on dataset D4.15 found that the 4P-LH was quantitatively a less good match to the data than that obtained for the Laplace distribution (D_{sp}=0.020 c.f D_{sp}=0.011). However, this is still within the 95% confidence limit (D_{sp}=0.055), and qualitatively the ripple around the perfect fit baseline on the DSP plot was reduced with the 4P-LH distribution fit (Figure 4), apart from the divergence near the lower bound of the peak which gives rise to the large value of D_{sp}. Despite the concerns, the fit was too good to reject the 4P-LH distribution without further testing.

Stable distribution

The Stable distributions are a class of wide-tailed distributions whose instances include the Gaussian and Lorentz distributions [17]. They are also known as Levy skew alpha stable distributions after Paul Lévy who was the first to characterise them. There are four parameters: an index of stability $0 < \alpha < 2$, skewness $-1 < \beta < 1$, scale $\gamma > 0$ and location δ. Alpha is two for a Gaussian and one for the Lorentz distribution. As alpha tends to zero the Stable distribution tends towards the Dirac delta function.

The Stable distribution is defined by a Fourier transform of its characteristic function (3), for which there are a several parameterisations (Table 1). Index α and skewness β are the same in all, but definitions of the scale γ and location δ parameters differ. The 1-parameterisation is favoured for demonstrating mathematical properties of the distribution, for example asymptotic behaviour. The 0-parameterisation, which is everywhere continuous, is recommended for numerical fitting and statistical inference [17]. However, for the current purpose the 2-parameterisation is preferred, as δ is defined to be the mode, in contrast to the 0 and 1 parameterisations where δ is less intuitively defined. As they are unfamiliar, the mathematical definitions of the parameterisations are given, but in practice Nolan's "STABLE" FORTRAN program [19] has been used to perform the Fourier transform computations, and the mechanics of the solution of these equations need not be considered any more than would the mechanics of the calculation of the error function when fitting a Gaussian or log-normal distribution. The equations have been rearranged from those given in Nolan [17, 22] in order to more clearly show the family resemblances and differences between the parameterisations.

The fit to screening dataset D4.15 (D_{sp}=0.005) is quantitatively slightly better than the Lorentz fit (D_{sp}=0.007), although the slight ripple around the perfect fit baseline on the DSP plot was still present (Figure 4). It was found that adequate initial parameter estimates could be made by inspection. The sensitivity of the DSP plot shows that the Stable distribution is in the small diameter limit not quite the correct description of the data. However, the plot also very clearly indicates that the Stable distribution is an exceptionally good model over the vast majority of the range of the data.

$$w(d) = \int_{-\infty}^{\infty} \varphi(t) e^{-itd} dd \qquad (3)$$

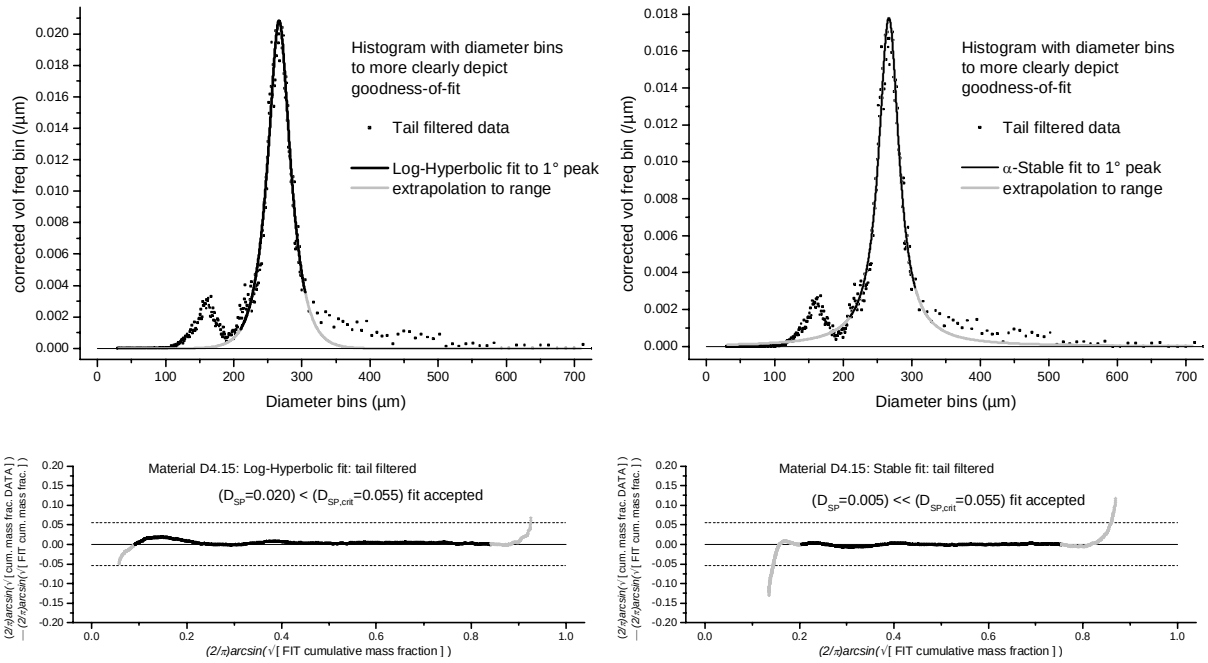

Figure 4. 4P-LH (left) and Stable (right) fits to (area-corrected) primary peak of dataset D4.15

Table 1. parameterisations of the Stable distribution

0-parameterisation	**1-parameterisation**	**2-parameterisation**
$\varphi(t)=\exp\left\{ it\delta-\gamma^{\alpha}\lvert t\rvert^{\alpha}\left[1-i\beta.sign(t).\Phi\right]\right\}$ $\left.\begin{aligned}\Phi&=\tan\left(\frac{\pi\alpha}{2}\right).\left[1-\gamma^{1-\alpha}\lvert t\rvert^{1-\alpha}\right]\\ \Phi&=-\frac{2}{\pi}\left(\ln\lvert t\rvert+\ln\gamma\right)\end{aligned}\right\}\begin{aligned}&\alpha\neq1\\&\alpha=1\end{aligned}$	$\varphi(t)=\exp\left\{ it\delta-\gamma^{\alpha}\lvert t\rvert^{\alpha}\left[1-i\beta.sign(t).\Phi\right]\right\}$ $\left.\begin{aligned}\Phi&=\tan\left(\frac{\pi\alpha}{2}\right)\\ \Phi&=-\frac{2}{\pi}\ln\lvert t\rvert\end{aligned}\right\}\begin{aligned}&\alpha\neq1\\&\alpha=1\end{aligned}$	$\varphi(t)=\exp\left\{ it(\delta-\alpha^{-1/\alpha}\gamma\,\Psi)-\gamma^{\alpha}\lvert t\rvert^{\alpha}\frac{1}{\alpha}\left[1-i\beta.sign(t).\Phi\right]\right\}$ $\left.\begin{aligned}\Phi&=\tan\left(\frac{\pi\alpha}{2}\right)\\ \Phi&=-\frac{2}{\pi}\ln\lvert t\rvert\end{aligned}\right\}\begin{aligned}&\alpha\neq1\\&\alpha=1\end{aligned}$ $\left.\begin{aligned}\Psi&=\beta\tan\left(\frac{\pi\alpha}{2}\right)+m(\alpha,\beta)\\ \Psi&=\beta\frac{2}{\pi}\ln\gamma+m(\alpha,\beta)\end{aligned}\right\}\begin{aligned}&\alpha\neq1\\&\alpha=1\end{aligned}$ Where m(α, β) is the mode of the standardised 0-parameterised distribution S(α, β, γ, δ: 0) = S(α, β, 1, 0: 0) which is found numerically

Testing fit functions against the multimodal distributions

If the observed secondary peaks at small sizes were truly solely due to either satellite droplet formation or orifice size variation, then they arise from the same physical mechanism as the primary peak, and a good fit function should be able to account for both primary atomisation and secondary satellite droplet peaks with meaningfully related parameters. Fitting to these bimodal data has been used as a demanding test to resolve which distribution function is the best model for the data.

An important property of the Stable distribution is self-similarity. If it really is a good description of the underlying physics, then the secondary peak should come from the same (α, β) family and vary only in the location parameter delta. Mathematically self-similarity would be satisfied if the scale parameter γ varied also, but physically it is postulated that the dispersion of the satellite droplet sizes should match the dispersion in primary droplet size, as both arise from the same atomisation event, so the width parameter γ should be the same. Hence in performing the bimodal fits α, β and γ have been constrained to be the same between primary and secondary peaks, and only the location parameter delta (which is defined to be the position of the mode) differs. Intuitively it is expected that γ would widen with increasing number of nozzles, and also that for a given fluid

with constant number and detailed mechanical construction of the nozzles, that the ratio of γ/δ should be constant as nozzle size (and hence δ) were varied. However, there are insufficient appropriately sequenced datasets available in this study to test these further postulates about γ.

Some datasets were found to have a secondary peak that was both too large in volume fraction and too close in diameter to the main peak to be convincingly attributed to satellite droplet formation, but was better described as variation between orifice sizes in the sprayplate. It is less defensible in this case that the Stable width parameter γ should be the same for each peak. One of the nozzle diameters will give a jet that is excited at resonance from the driving frequency, and will have the value of γ characteristic of the resonant jet breakup. Another jet emerging from the same sprayplate, driven at the same frequency, but from an orifice of different diameter, is unlikely to also be at resonance, and thus γ might be expected to be larger. It was indeed found that γ chosen for the primary peak was not often an excellent fit to the secondary peak, but in only one case (dataset D7.7) was the value of γ fitted to the primary peak not an acceptable fit against the secondary peak. It was, however, acceptable for $\gamma_2/\gamma_1 = \delta_2/\delta_1$.

In contrast to the Stable distribution, it is unclear how the parameters of the 4-parameter log-hyperbolic distribution should be related between the primary and secondary peaks, as the parameters have less intuitive physical meanings.

Tertiary peaks at large diameter have been postulated to be artefacts due to agglomeration. The agglomeration process is independent from the atomisation, so self-similarity with the primary atomisation peak is not expected: it is not even clear that it should follow the same type of distribution. Thus the multi-peak analysis has been confined to bimodal primary mode atomisation and the secondary mode at smaller diameter.

When performing the bimodal fits, the volume ratio between the two peaks was first estimated by inspection, and subsequently adjusted if necessary.

Comparing the example fits shown in Figure 5, both the 4-parameter log-hyperbolic and the Stable distribution appear[1] on inspection to fit the data reasonably, although both show some ripple around the baseline in the DSP plot, indicating that neither fit is perfect. Neither distribution function bottoms the trough around 200µm between the peaks. The Stable distribution underestimates significantly the cluster of datapoints just greater than 200µm. The 4-parameter log-hyperbolic distribution produces numerically the better fit, but the Stable distribution is more compelling in the maintenance of self-similarity in the values of the parameters between the peaks: a better agreement than that shown could be obtained by the artifice of letting the α, β, γ parameters float between peaks as was permitted for α, β, δ in the 4P-LH fit.

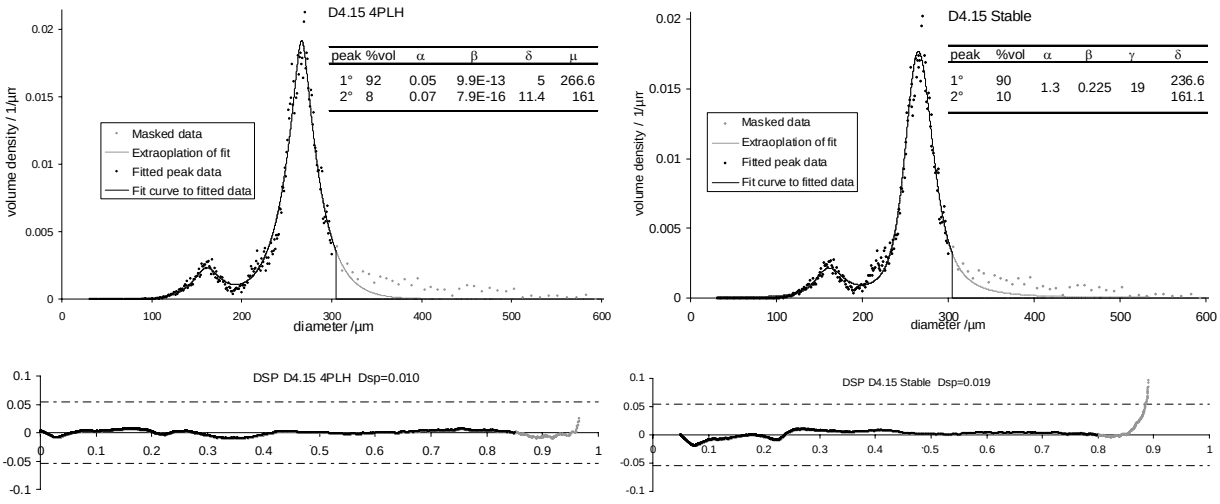

Figure 5. bimodal 4P-LH (left) and Stable (right) fits to dataset D4.15

Stable distribution fits to all datasets

The Stable distribution fits were for almost all the datasets found to be both qualitatively and quantitatively better than the 4-parameter log-hyperbolic distribution, and the fit parameters are always less arbitrary, especially when applied to the bimodal distribution cases when the assumption of self-similarity of the distribution between the primary atomisation and secondary satellite droplet peaks works consistently for the Stable distribution, but erratically for the 4-parameter log-hyperbolic distribution.

Stable fit parameters, the D_{sp} goodness-of-fit statistic and the comparison with the 95% confidence level limiting value for all size distribution datasets in this study are summarised in Table 2. With bimodal fits, only parameters that differ for the secondary peak are tabulated. The D_{sp} statistic is tabulated for both peaks

individually, and also for the combined fit to both peaks. Peak upper and lower limits are explicit where the fit is to a subset of the data. The lower bound of the secondary peak is normally the dataset minimum, in which case the value appears in brackets. In five cases, however, the smallest diameter data was discordant even with a bimodal fit, and the secondary peak lower bound was chosen to be greater than the dataset minimum. In these cases, the D_{sp} statistic is shown for both the fit within the selected limits, and also from the dataset minimum.

In all cases the agreement of the Stable distribution model with the data is acceptable at the 95% confidence level, and in most cases it is a comfortably small fraction of the limit. The borderline fit of datasets D10.6 and D11.4 is attributed to agglomeration: as indicated by the values in Table 2, when the largest sieve data are excluded (10 and 20% of the total volume for each dataset respectively), the concordance is comfortably within the confidence limits in both cases. For the bimodal fits, the D_{sp} statistic for each peak in isolation is often relatively poor compared to the D_{sp} value for the fit to the combined peaks. This is an artefact of the selection of the bounds. The assumption was made that bounds could be chosen by inspection such that the contribution from other peaks was trivial. In many cases, the peaks are too closely spaced for this assumption to be valid, and with the bounds are set sufficiently wide to be able to meaningfully gauge the quality of the fit, there are contributions from other peaks. It should be noted, however, that even if poor by comparison, the D_{sp} statistic is still always within the 95% confidence limits, even for the peaks in isolation.

Trend in Stable alpha parameter with feed liquor viscosity

Unusually for a spray size distribution, which are normally right skewed, the PDA data for the low viscosity system of water and Materials C were found to be good fits to the symmetrical Normal distribution (a Stable distribution with α=2). Materials D had higher viscosity, and the alpha parameter is observed to be smaller. Surprisingly, it is indicated in Figure 6 that the Stable alpha parameter is roughly correlated with the viscosity of the liquid feed to the Acoustic Atomiser. A linear regression line has been plotted, not because the trend is necessarily supposed to be linear, but because there are many coincident datapoints, which lessen the visual impression of the trend. The viscosity data are the shear viscosity at the nozzle wall shear rate. I have reported elsewhere that atomisation behaviour is best mapped by extensional viscosity [12]. That conclusion had not been made when these experiments were performed, and the extensional viscosity data cannot now be measured. However, it is expected that the extent of strain hardening would be similar and not significant for all Materials D, which show the greatest range of viscosity in Figure 6. Thus the use of shear viscosity data instead of extensional viscosity data may not be rigorous but should not alter the validity of the conclusion.

The linear regression excludes the Material A and dataset C3 production plant data, which are outliers from the trend of decreasing alpha with increasing viscosity,. The most satisfactory explanation is increased dispersion in the size distribution as the result of manufacturing tolerance in size of holes, where the overall size distribution is an ensemble of several hundred individual nozzle size distributions, each with a slightly different mean and width. Intriguingly and somewhat counter-intuitively, it was found that although α decreases for the large scale atomisers, the width measured as the ratio of the 95^{th} percentile to the mode of the volume distribution does not increase.

A physical rationalisation can be made for the decrease in the stable alpha parameter with increasing liquid viscosity in these resonance jet break-up nozzles. The Lorentz distribution function (Stable α=1) is the solution in the frequency domain of the equations of motion for a damped harmonic oscillator excited by a resonant sinusoidal fluctuation. This system is highly underdamped (otherwise the initial perturbation would decay, rather than being amplified along the jet until droplets broke off). As the viscosity (and hence the damping) increases, the system becomes progressively less like an undamped simple harmonic oscillator, and more like an ideal damped harmonic oscillator.

Conclusions

A selection of distribution functions has been tested against forty Acoustic Atomiser droplet and particle size distribution datasets, covering a range of materials, with mean sizes varying over two orders of magnitude and flowrate ranging over four orders of magnitude. Although it has not previously been reported for use in droplet size distributions, the Stable distribution has been found in this research to be a better fit to the Acoustic Atomiser size distribution data than any of the fit functions commonly reported in the sprays literature.

It is proposed that the Stable distribution is not only a good numerical fit to the data, but furthermore that it is in some way descriptive of the physics of atomisation. The trend in alpha towards the Gaussian limit $\alpha = 2$ for inviscid liquids and towards the Lorentz limit of $\alpha = 1$ as the feed viscosity increases, is consistent with the physical description as a simple or damped forced resonator respectively

Acknowledgements

It is a pleasure to thank AkzoNobel for funding this research, colleagues at AkzoNobel who provided the size distribution data, and John Nolan for the STABLE program and pre-publication chapters from [17].

References

[1] Masters, K., *Spray Drying Handbook*, 5th ed., Longman, 1991, pp. 4, 195-196.
[2] Oakley, D. E., *Chem. Engg. Progress* 93:48-54 (1997).
[3] van Dycke, F., *Designing, optimising and controlling spray drying processes,* Ede, The Netherlands, 21-22 Sept 2006.
[4] Bartels, J., *Designing, optimising and controlling spray drying processes,* Ede, The Netherlands, 21-22 Sept 2006.
[5] Rayleigh, *Proc. London Math. Soc.* 10:4-13 (1878).
[6] Rayleigh, *Proc. Royal Society* 29:71-97 (1879).
[7] Oliver, R., Fairclough, A. R. N., Antonini, A. M., Munro, R. J., Lipscombe, L. W., WO9420204 (1994).
[8] Oliver, R., Lloyd-Jones, G. N., EP0320153 (1993).
[9] Fiannaca, C., Threlfall-Holmes, P., WO 2005/058473 (2005).
[10] Threlfall-Holmes, P., *Solids drying in theory and practice,* IChemE Particle Technology Subject Group Meeting, UCL, 2 April 2008.
[11] Threlfall-Holmes, P., Fiannaca, C., Oliver, R., *19th Annual meeting of ILASS (Europe),* Nottingham, UK, 6-8 September, 2004, p. K3.
[12] Threlfall-Holmes, P., PhD thesis, Heriot-Watt University, 2009.
[13] Lloyd, E., *Handbook of applicable mathematics, Volume VI part B: Statistics, Vol. VI Part B*, Wiley-Interscience, 1984, pp. 606-611.
[14] Bousfield, D. W., Keunings, R., Marrucci, G., Denn, M. M., *J. Non-Newtonian Fluid Mech.* 21:79-97 (1986).
[15] Clasen, C., Eggers, J., Fontelos, M. A., Li, J., McKinley, G. H., *J. Fluid Mech.* 556:283 - 308 (2006).
[16] Michael, J. R., *Biometrika* 70:11-17 (1983).
[17] Nolan, J. P., *Stable distributions - models for heavy tailed data*, Birkhäuser, 2009.
[18] Pollard, J. H., *A handbook of numerical and statistical techniques*, CUP, 1977, pp. 151-155.
[19] Nolan, J. P., *Commun. Statist. - Stochastic Models* 13:759-774 (1997).
[20] Stanton, D. W., Senecal, P. K., Hung, C. C., Rutland, C. J., Reitz, R. D., *Atomization and Sprays* 8:363-392 (1998).
[21] Xu, T.-H., Durst, F., Tropea, C., *Atomization and Sprays* 3:109-124 (1993).
[22] Nolan, J. P., *Statistics and Probability Letters* 38:187-195 (1998).

Table 2. summary of Stable distribution fit parameters for all datasets

Dataset		Stable (2-parameterisation) fits to primary atomisation peaks										2° satellite peak							Bimodal Dsp			
	Sizing	Extent of fit			parameters				Dsp			Extent		params		Dsp		v ratio	from			
	method		dL	dU	α	β	γ	δ	fit	limit	%limit	dL	dU	γ_2	δ_2	fit	%limit	1°:2°	min	%limit	dL2°	%limit
average of data																						
Water A	PDA	1° peak	(22.2)	67.3	**2**	n/a	4	42.3	0.050	0.154	32%											
Water B	PDA	All data			**2**	n/a	5.28	274.84	0.006	0.168	4%											
A1	sieve	All data			**1.5**	0.2	337	2630	0.045	0.100	45%											
A2	sieve	All data			**1.65**	0.6	250	2590	0.035	0.082	43%											
A3	sieve	All data			**1.5**	0.5	300	2630	0.057	0.080	71%											
B	sieve	All data			**1.91**	0	69.0	557	0.017	0.149	11%											
C1	PDA	All data			**2**	n/a	13	291.3	0.119	0.132	90%											
C2	PDA	1° peak	(33)	65	**2**	n/a	1.28	43.8	0.091	0.132	69%											
C3	PDA	All data			**1.7**	0.3	12	238	0.062	0.145	43%											
D1.17a	sieve	All data			**1.95**	0.5	80	410	0.100	0.158	63%											
D1.17b	sieve	All data			**1.9**	0.25	60	550	0.020	0.168	12%											
D1.23	sieve	All data			**1.8**	0.3	90	425	0.032	0.168	19%											
D1.25	sieve	All data			**1.9**	0.25	130	590	0.034	0.168	20%											
D1.26	sieve	All data			**1.9**	0.3	90	570	0.021	0.168	13%											
D1.28	sieve	All data			**1.6**	0.25	80	470	0.044	0.168	26%											
D1.30	sieve	All data			**1.9**	0.5	105	425	0.050	0.168	30%											
D3.7	Visisize	bimodal	190	300	**1.49**	0.72	45.0	255.1	0.0232	0.0548	42%	90	165	155		0.0170	31%	90:10	0.0137	25%	0.0153	4%
D3.8a	Visisize	bimodal	200	290	**1.6**	0.25	35	250	0.0285	0.0548	52%	70	200	190		0.0187	34%	76:24	0.0135	25%	0.0145	3%
D3.8b	Visisize	bimodal	200	290	**1.6**	0.25	35	254	0.0280	0.0548	51%	65	190	192		0.0164	30%	79:21	0.0169	31%	0.0109	2%
D3.9	Visisize	1° peak	80	280	**2**	n/a	47.7	221	0.0134	0.0548	24%											
D3.10	Visisize	1° peak	165	262	**1.35**	0	19.1	236.7	0.0072	0.0548	13%											
	Visisize	bimodal	150	262	**1.27**	0.25	20.5	235.4	0.0050	0.0548	9%	90	150	129		0.0132	24%	98:2	0.0150	27%	0.0054	6%
D4.15	Visisize	1° peak	210	305	**1.01**	0	18.0	266.6	0.0054	0.0548	10%											
	Visisize	bimodal	240	305	**1.3**	0.225	18.3	265.33	0.0042	0.0548	8%	(31)	180	161		0.043	78%	90:10	0.0190	35%		
D4.16	Visisize	1° peak	220	300	**1.34**	0	25.6	269.3	0.0048	0.0548	9%											
	Visisize	bimodal	210	310	**1.3**	0.225	25.5	267.47	0.0046	0.0548	8%	70	190	177		0.0205	37%	96:4	0.0178	32%	0.0118	14%
D7.3a	Visisize	1° peak	210	365	**1.6**	0	45.1	283.7	0.0051	0.0548	9%											
	Visisize	bimodal	235	370	**1.6**	0.9	40	283.1	0.0151	0.0548	28%	(31.8)	190	200		0.0143	26%	87:13	0.0093	17%		
D7.5a	Visisize	bimodal	240	325	**1.6**	0.65	33	277	0.0202	0.0548	37%	(68.2)	205	204		0.0175	32%	68:32	0.0129	24%		
D7.5b	Visisize	bimodal	230	330	**1.6**	0.3	43	290	0.0401	0.0548	73%	(31)	205	204		0.0164	30%	69:31	0.0115	21%		
D7.6a	Visisize	bimodal	250	350	**1.6**	0.3	37	280	0.0148	0.0548	27%	(31)	205	206		0.0213	39%	76:24	0.0149	27%		
D7.6b	Visisize	bimodal	250	360	**1.6**	0.9	45	285	0.0179	0.0548	33%	(31.8)	205	205		0.0183	33%	68:32	0.0128	23%		
D7.7	Visisize	bimodal	250	360	**1.6**	0.5	45	297	0.0098	0.0548	18%	(31.8)	205	210	30	0.0120	22%	88:12	0.0130	24%		
D7.9	Visisize	bimodal	365	340	**1.7**	0.3	32	285	0.0113	0.0548	21%	(32.5)	240	221		0.0171	31%	52:48	0.0139	25%		
D7.10	Visisize	bimodal	260	360	**1.6**	0.5	35	305	0.0352	0.0548	64%	(34)	250	215		0.0188	34%	61:39	0.0097	18%		
D8.9a	Visisize	bimodal	270	390	**1.3**	0.3	34	330	0.0184	0.0548	34%	(31)	230	190		0.0348	63%	71:29	0.0208	38%		
D8.10a	Visisize	bimodal	285	390	**1.2**	0.75	42	330	0.0206	0.0548	38%	(31)	230	186		0.0241	44%	71:29	0.0142	26%		
D8.11a	Visisize	bimodal	270	390	**1.32**	0.6	40	325	0.0294	0.0548	54%	(31.8)	230	180		0.0248	45%	69:31	0.0183	33%		
D8.12a	Visisize	bimodal	270	330	**1.3**	0.5	38	330	0.0134	0.0548	24%	(31)	230	187		0.0324	59%	74:26	0.0186	34%		
D10.3	sieve	All data			**1.9**	0.25	70	280	0.065	0.145	45%											
D10.5	sieve	All data			**2**	0	31	375	0.058	0.138	42%											
D10.6	sieve	All data			**2**	0	43	300	0.144	0.145	99%											
		1° peak	(0)	350					0.038		26%											
D11.3	sieve	1° peak	(0)	250	**1.9**	0.25	62	318	0.02	0.154	13%											
D11.4	sieve	All data			**1.9**	0.25	62	318	0.127	0.130	98%											
		1° peak	(0)	355					0.039		30%											

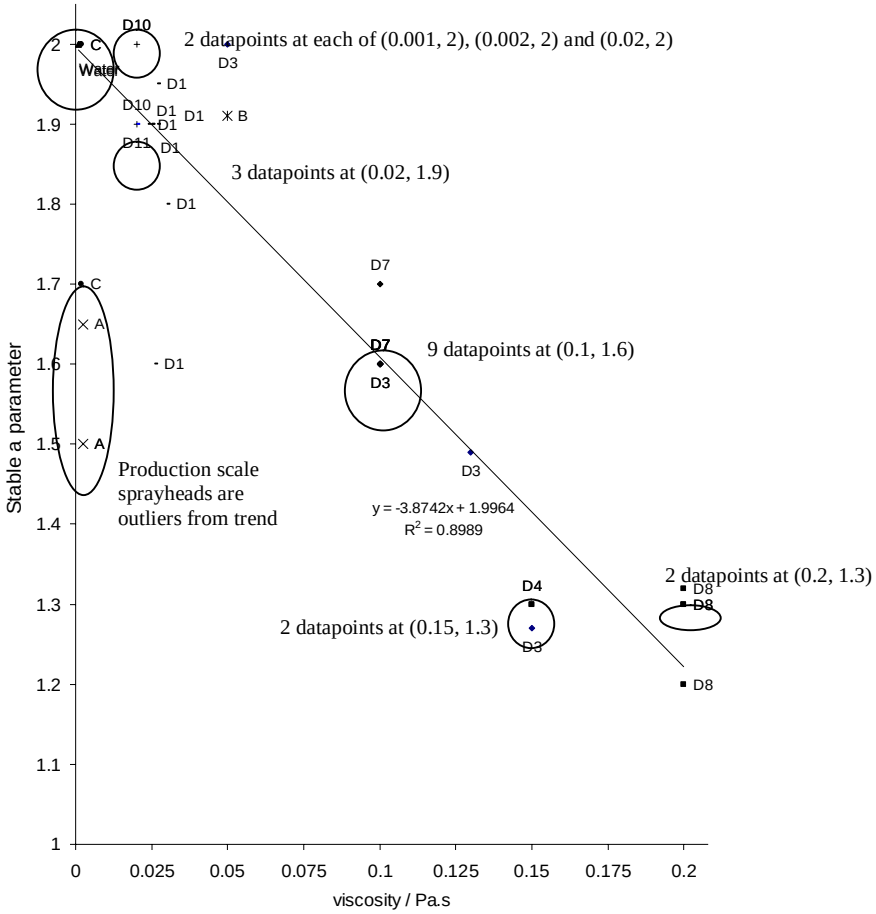

Figure 6. trend in Stable distribution α parameter with atomiser liquid feed viscosity